Published in final edited form as:

Ultrasound Med Biol. 2019 March ; 45(3): 846–858. doi:10.1016/j.ultrasmedbio.2018.12.001.

CONTROL OF ACOUSTIC CAVITATION FOR EFFICIENT SONOPORATION WITH PHASE-SHIFT NANOEMULSIONS

Mark T. Burgess[*,1], **Tyrone M. Porter**[*,†]

[*]Department of Mechanical Engineering, Boston University, Boston, Massachusetts, USA;

[†]Department of Biomedical Engineering, Boston University, Boston, Massachusetts, USA

Abstract

Acoustic cavitation can be used to temporarily disrupt cell membranes for intracellular delivery of large biomolecules. Termed *sonoporation*, the ability of this technique for efficient intracellular delivery (*i.e.*, >50% of initial cell population showing uptake) while maintaining cell viability (*i.e.*, >50% of initial cell population viable) has proven to be very difficult. Here, we report that phase-shift nanoemulsions (PSNEs) function as inertial cavitation nuclei for improvement of sonoporation efficiency. The interplay between ultrasound frequency, resultant microbubble dynamics and sonoporation efficiency was investigated experimentally. Acoustic emissions from individual microbubbles nucleated from PSNEs were captured using a broadband passive cavitation detector during and after acoustic droplet vaporization with short pulses of ultrasound at 1, 2.5 and 5 MHz. Time domain features of the passive cavitation detector signals were analyzed to estimate the maximum size (R_{max}) of the microbubbles using the Rayleigh collapse model. These results were then applied to sonoporation experiments to test if uptake efficiency is dependent on maximum microbubble size before inertial collapse. Results indicated that at the acoustic droplet vaporization threshold, R_{max} was approximately 61.7 ± 5.2, 24.9 ± 2.8, and 12.4 ± 2.1 μm at 1, 2.5 and 5 MHz, respectively. Sonoporation efficiency increased at higher frequencies, with efficiencies of 39.5 ± 13.7%, 46.6 ± 3.28% and 66.8 ± 5.5% at 1, 2.5 and 5 MHz, respectively. Excessive cellular damage was seen at lower frequencies because of the erosive effects of highly energetic inertial cavitation. These results highlight the importance of acoustic cavitation control in determining the outcome of sonoporation experiments. In addition, PSNEs may serve as tailorable inertial cavitation nuclei for other therapeutic ultrasound applications.

Keywords

Sonoporation; Drug delivery; Microbubbles; Ultrasound; Acoustic cavitation; Inertial cavitation

Address correspondence to: Tyrone M. Porter, Department of Mechanical Engineering, Boston University, 110 Cummington Mall, Boston, MA 02215, USA. tmp@bu.edu.

[1]Present address: Department of Biomedical Engineering, Columbia University, 351 Engineering Terrance, 1210 Amsterdam Avenue, New York, NY 10027, USA.

INTRODUCTION

The cell membrane inhibits intracellular delivery of numerous large bioactive agents including DNA, RNA, proteins and drugs. Ultrasound-stimulated microbubble activity (*i.e.*, acoustic cavitation) has been reported to permeabilize cell membranes for bioactive agent delivery in a process termed *sonoporation* (Lentacker et al. 2014). Sonoporation relies on the ability of oscillating microbubbles to generate stresses at the cellular level through microstreaming and or rapid microbubble expansion and collapse (Coussios and Roy 2008; Leighton 1994; Lentacker et al. 2014; Neppiras 1980; Zhou et al. 2012). As the gatekeeper to the interior of the cell, the cell membrane's integrity can be compromised by mechanical forces generated near the cell during acoustic cavitation (Fan et al. 2012; Kudo et al. 2009; Ohl et al. 2006; Wamel et al. 2006; Zhou et al. 2009). This process can be reversible or irreversible (*i.e.*, leading to cell death) depending on the intensity and duration of activity (Hallow et al. 2006; Lai et al. 2006).

Depending on the application, the definition of efficient delivery may vary depending on the desired outcome. Delivery of a payload to a large fraction of the initial cell population may be necessary for agents that utilize cellular machinery, such as DNA, RNA and proteins. The goal in this scenario was to achieve high intracellular delivery with minimal cell death (*e.g.*, genetic modification or cellular reprogramming). Alternately, it may be beneficial to destroy a large fraction of the cell population and achieve delivery to the remaining viable cells (*e.g.*, drug delivery to cancer cells). A retrospective review and analysis of documented sonoporation studies by Liu et al. (2012) concluded that sonoporation has been an inefficient method for delivery of biomolecules to cultured cells *in vitro* (*i.e.*, did not achieve delivery to >50% of the initial cell population) without significant cell death (*i.e.*, >50% of the initial cell population killed during sonoporation). This has been a major hurdle in the use of sonoporation, and researchers have begun to address this issue with careful experimental design and cavitation control (Burgess and Porter 2015; Carugo et al. 2015; Dixon et al. 2013; Fix et al. 2017; Sengupta et al. 2014; Seya et al. 2015; Song et al. 2015).

A recent study by Burgess and Porter (2015) achieved high sonoporation efficiency with the use of phase-shift nanoemulsions (PSNEs) as acoustic cavitation nuclei. PSNEs are liquid perfluorocarbon (PFC) nanoparticles that can change phase from liquid to vapor when exposed to ultrasound in a process called *acoustic droplet vaporization* (ADV) (Kripfgans et al. 2000). By using a passive cavitation detector (PCD) during their sonoporation experiments, Kripfgans et al. detected broadband acoustic emissions indicative of inertial cavitation throughout the ultrasound exposure. This acoustic cavitation activity was found to permeabilize cell membranes for uptake of a large biomolecule in a dose-dependent manner (*i.e.*, increasing uptake with increasing inertial cavitation activity). Although cell viability decreased with increasing cavitation activity, cell death was minimal at optimal experimental parameters (*i.e.*, >80% cell viability). In general, inertial cavitation is associated with erosive and damaging effects that can be detrimental to cells (Hallow et al. 2006; Lai et al. 2006; Sundaram et al. 2003). Therefore, we proposed to further explore the role inertial cavitation has in sonoporation efficiency with PSNEs. Ultrasound frequency and pressure are the two most critical parameters that affect the intensity of inertial cavitation, as predicted by acoustic cavitation theory (Apfel 1981; Apfel and Holland 1991; Holland and Apfel 1989).

Consequently, exploring the frequency-dependent effects of ADV of PSNEs, could provide insight into the high cell viability measured in the study conducted by Burgess and Porter (2015). The authors used a 5-MHz transducer in the study, which is a higher frequency than traditionally has been used in sonoporation studies (i.e. f ≤ 1 MHz) (Liu et al. 2012). We hypothesized that the microbubble dynamics of inertial cavitation nucleated from PSNEs, and thus sonoporation efficiency, were a function of ultrasound frequency.

In this study, we used a broadband PCD to capture frequency-dependent acoustic emissions from individual microbubbles derived from PSNEs at the ADV threshold. Short pulses of ultrasound were used throughout the study to elicit a transient microbubble response. By analyzing the time traces of the PCD, we were able to approximate the extent of microbubble expansion (R_{max}) and, therefore, the intensity of inertial collapse. These results were then applied to sonoporation experiments to test if the approximated R_{max} was related to the sonoporation efficiency. We hypothesized that lower frequencies would allow microbubbles to achieve a larger R_{max} because of the longer rarefactional periods of the ultrasound wave, thus giving the microbubble more time to grow and store energy during expansion. This should lead to a decrease in sonoporation efficiency caused by excessive cellular damage on inertial collapse. In the sections that follow, we detail how PSNEs were fabricated and how the bubble dynamics post-vaporization were examined. In addition, the details of frequency-dependent sonoporation experiments are presented along with definitions of uptake, viability and uptake efficiency for direct comparison of results between different ultrasound frequencies and frequency-dependent bubble dynamics. Finally, the results of the study are presented along with a detailed discussion of the frequency-dependent acoustic cavitation properties of PSNEs in relationship to sonoporation efficiency.

METHODS

Phase-shift nanoemulsions

Phase-shift nanoemulsions were fabricated using a three-step hydration, sonication and extrusion procedure (Burgess and Porter 2015; Kopechek et al. 2012). The stabilizing phospholipid shell of the PSNEs consisted of 1,2-dipalmitoyl-*sn*-glycero-3-phosphocholine and 1,2-distearoyl-*sn*-glycero-3-phosphoethanolamine-*N*-[methoxy(polyethylene glycol)-2000] (ammonium salt) (DSPE-mPEG2000) (Avanti Polar Lipids, Alabaster, AL, USA) at a 9:1 molar ratio. The lipids were weighed out in a 7-mL glass vial and dissolved in a small amount of chloroform (Sigma-Aldrich, St. Louis, MO, USA). The chloroform was slowly evaporated with a stream of argon to leave the residual lipid film on the side of the vial. The remaining chloroform was removed by placing the vial in a vacuum desiccator overnight. The lipid film was subsequently hydrated with phosphate-buffered saline (PBS) (Boston Bioproducts, Ashland, MA, USA) and placed in a 50°C water bath for 1 h with periodic mixing and sonication in an ultrasonic bath (Cole-Parmer, Vernon Hills, IL, USA). The solution of lipid vesicles was then sonicated with a high-power sonication tip (Sonic & Materials, Newtown, CT, USA) for 1 min to produce a clear solution of small lipid vesicles at a lipid concentration of 1 mg/mL.

Phase-shift nanoemulsions were fabricated by adding 100 μL of perfluoropentane (PFP, 29°C boiling point) (Synquest Labs, Inc., Alachua, FL, USA) or perfluorohexane (PFH, 55°C boiling point) (Synquest Labs, Inc.) to 3 mL of the lipid solution and sonicating with a high-power sonication tip (Sonics & Materials, Inc.) while the vial was partially submerged in an ice water bath. To prevent heating, a pulsing regime of 10 s on, 20 s off, for a total on time of 1 min, was used. This opaque suspension was then added to 7 mL of cold PBS and pressure extruded 10 times through two stacked 200-nm polycarbonate filters using an extruder (LIPEX, Northern Lipids Inc., Burnaby, BC, Canada). Excess lipid vesicles were removed by three centrifugal washes for 5 min at 3000*g*, and then the PSNE pellet was resuspended with PBS. PSNEs were stored at 4°C and used for up to a week.

Tunable resistive pulse sensing with the qNano (Izon Science Ltd., Cambridge, MA, USA) was used to determine the size and concentration of PSNEs. The qNano allows particle-by-particle counting and sizing of submicron particles as they pass through a stretchable nanopore. A NP200 nanopore (diameter range: 100–400 nm) was used along with 200-nm carboxylated polystyrene standards of known size and concentration for calibration. The PSNEs were diluted 1000-fold in filtered PBS, and at least 1000 nanopore blockade events were recorded at three different pressure-driven flow regimes according to the manufacturer's instructions. This was repeated with 200-nm standards using the same instrument settings to determine the size and concentration of PSNEs.

Acoustic droplet vaporization threshold

The vaporization of PSNEs as a function of peak negative pressure and frequency was investigated using the experimental arrangement illustrated in Figure 1a. A PSNE suspension was sonicated with a focused ultrasound (FUS) transducer submerged in a degassed water bath heated to 37°C (Fig. 1a). A broadband (0.015–15 MHz), cylindrically focused transducer (Y-102, Sonic Concepts) was used as a PCD and positioned perpendicular to and confocally with the FUS transducer. Three FUS transducers were used to sonicate the PSNE suspension at center frequencies of 1 MHz (H-102, Sonic Concepts, Bothell, WA, USA), 2.5 MHz (H-108, Sonic Concepts) and 5 MHz (SU-108, Sonic Concepts). Free-field pressure calibrations of each FUS transducer at the focal point were performed with a 75-μm needle hydrophone (Precision Acoustics, Dorchester, Dorset, England). Peak negative pressure measurements were made up to 1 MPa and then extrapolated out to higher pressures using a linear fit. The transducers were driven using a 55-dB radiofrequency power amplifier (Electronics & Innovation, Rochester, NY, USA) and waveform generator (Agilent Technologies Inc., Santa Clara, CA, USA). PSNEs were diluted into partially degassed (~30% dissolved oxygen), de-ionized water inside a custom-made enclosure with weakly attenuative sides (Tegaderm, 3M, St. Paul, MN, USA) at a concentration of 10^9 PSNEs/mL. The enclosure was submerged into the heated water bath, and a magnetic stir bar was placed inside for mixing of PSNEs during the experiments.

The peak negative pressure threshold for ADV of PSNEs at each frequency was determined by sonicating the PSNE suspension with FUS pulses at a 100-Hz pulse repetition frequency. A peak negative pressure range of 4 to 8 MPa was used for each ultrasound frequency. At each pressure step, the output from the PCD was routed through a 15-MHz low-pass filter

(Allen Avionics Inc., Mineola, NY, USA), pre-amplified 40 dB (Model DHPVA-100, Femto, Berlin, Germany) and digitized at 50 MS/s with a 14-bit oscilloscope board (GaGe Corp., Lockport, IN, USA). A total of 100 individual time traces were captured at each pressure step for post-processing. A custom MATLAB (The MathWorks, Natick, MA, USA) program was used for instrument control and automation of data collection and analysis. ADV of PSNEs was determined by defining a voltage threshold within the gated region of the PCD time trace corresponding to acoustic emissions emanating from the focal zone of the FUS transducer based on time of flight. Below the ADV threshold, the PCD signal contained low-amplitude reflections from interfaces along the FUS path. When the ADV threshold was reached, the PCD signal amplitude within the gated region increased by more than 10-fold because of active scattering of the incident FUS pulse by the newly created microbubbles, thus confirming an acoustic cavitation event had occurred. The data for each pressure step were defined as the percentage of signals containing a cavitation event and plotted versus peak negative pressure. A sigmoidal function was used to fit the data in a manner similar to that used in previous studies identifying the acoustic cavitation threshold of micron-sized PFC droplets (Fabiilli et al. 2009). For the purpose of this study, we sought to approximate a pressure threshold for each frequency and then select a single pressure exceeding the threshold at all frequencies for the subsequent sonoporation study.

We define acoustic cavitation event and ADV of PSNEs interchangeably, because a cavitation event could also result from the host liquid or any other stabilized gas bodies present. Control experiments without PSNEs were performed in partially degassed (~30% dissolved oxygen), de-ionized water to identify the baseline amount of cavitation in the host liquid. Additional control experiments were performed with PFH PSNEs, which reportedly have a higher ADV pressure threshold than PFP PSNEs (Zhang and Porter 2010). Therefore, they serve as a control to ensure that cavitation events are not originating at the interface between the PSNEs and host liquid.

Analysis of acoustic emissions from individual microbubbles

Methods similar to that of Ammi et al. (2006) were employed to analyze the acoustic emissions from individual PSNEs during and after ADV. Temporal features of the PCD signal were analyzed to provide information about microbubble growth, collapse and rebound. Inferences were made about microbubble dynamics after ADV and its relationship to excitation frequency.

Passive cavitation detector signals from each frequency were analyzed at the pressure that resulted in ~10% of the PCD signals having an acoustic cavitation event. This allowed time traces of individual ADV events to be examined. In Figure 2a is an example PCD signal from the ADV of PSNEs using 1-MHz ultrasound at a peak negative pressure of 5.6 MPa. Intra-excitation emissions are defined as acoustic emissions that occur during the passage of the excitation waveform, whereas post-excitation emissions occur after the transmitted excitation waveform has propagated through the PCD focal volume. Because these emissions occur after the excitation waveform has passed, they are hypothesized to arise from the inertial collapse and rebound of the newly formed microbubble (Fig. 2b). The temporal features of the PCD time traces were used to estimate R_{max} using the Rayleigh

collapse model. This model considered the collapse of an empty cavity (no gas or vapor) located inside an incompressible fluid (Leighton 1994; Rayleigh 1917). The maximum radius, R_{max}, is defined as

$$R_{\max} = \frac{t_c\sqrt{P_0/\rho}}{0.915} \quad (1)$$

where t_c, P_0 and ρ are the collapse time, hydrostatic pressure and liquid density, respectively. As stated by Neppiras (1980), this is the simplest model for a collapsing spherical cavity, and all transient cavities start their collapse like this and, hence, are called Rayleigh-like. Equation (1) was used to predict the maximum radius of the microbubbles after ADV by equating the time delay between the intra-excitation and first post-excitation emission as $2t_c$, as illustrated in Figure 2b.

Frequency-dependent sonoporation

The experimental methods in this section follow the conventions put forth by Liu et al. (2012). A suspension of cells containing PSNEs and fluorescein isothiocyanate–dextran (FITC–dextran, average molecular weight: 20 kDa, Sigma-Aldrich) was exposed to FUS at a peak negative pressure of 6.5 MPa, which was above the ADV threshold of PSNEs for all frequencies. Flow cytometry analysis after the ultrasound exposure was used to determine the sonoporation efficiency at the three FUS frequencies. A cell proliferation assay was also performed 24 hr post-FUS exposure as another metric of cell viability and provided information on how well the cells recover over time. Lastly, mock exposures were performed in the setup described in Figure 1a using the same FUS parameters to characterize the acoustic cavitation activity during sonoporation experiments.

Sonoporation experiments were conducted using an experimental system similar to our previous work (Burgess and Porter 2015). As illustrated in Figure 1b, the system consisted of an FUS transducer submerged in a partially degassed, de-ionized water bath heated to 37°C. A three-axis micrometer positioning system (ThorLabs Inc., Newton, NJ, USA) was used to manipulate the FUS transducer position and place the focus within the cell suspension. The cell suspension was housed in a 1.5-mL polypropylene microcentrifuge tube and submerged into the water bath. This provided a sterile environment inside the tube, while providing an acoustic path for transmission of FUS into the suspension. Focal placement was achieved by using micron-sized PFC droplets for visualization of the resultant bubble cloud after ADV.

The same three FUS transducers used for determining the ADV threshold of PSNE were used for sonoporation experiments. A 55-dB radiofrequency power amplifier (Electronics & Innovation) and waveform generator (Agilent Technologies Inc.) were used to drive the transducers. The ultrasound parameters were 5-cycle pulses, 6.5-MPa peak negative pressure, 250-Hz pulse repetition frequency and 100-s treatment duration. The peak negative pressure used for these experiments was above the ADV threshold for all frequencies and resulted in consistent ADV of PSNEs (*i.e.*, 100% of the PCD signals contained cavitation events). Pressure calibrations of the FUS transducers were carried out with a modified

microcentrifuge tube to compensate for the attenuation. A program written in MATLAB was used for instrument control and automation of sonoporation exposures.

Human breast adenocarcinoma cells (MDA-MB-231) were grown to confluence in 75-cm^2 tissue culture flasks. Dulbecco's Modification of Eagle's Medium (DMEM, MediaTech Inc., Manassas, VA, USA) was used as the base culture medium and supplemented with 10% fetal bovine serum (Atlanta Biologics Inc., Flowery Branch, GA, USA), 2% L-glutamine (MediaTech Inc., Manassas, VA, USA) and 1% penicillin streptomycin (MediaTech Inc.). Cells were harvested using trypsin-EDTA (MediaTech Inc.) and counted using a hemocytometer (Hausser Scientific, Horsham, PA, USA). Cell culture medium without fetal bovine serum was used to re-suspend cells, and aliquots of 250,000 cells (19 μL) were added to 1.5-mL microcentrifuge tubes and incubated at 37°C. Before FUS exposure, cells were mixed with PSNEs (1 μL) and FITC–dextran (5 μL), which resulted in concentrations of 10^9 PSNEs/mL and 10 μM FITC–dextran, respectively.

By use of the same experimental system to examine the acoustic emissions of individual PSNEs (Fig. 1a), mock sonoporation exposures were performed using the same FUS parameters and PSNE concentrations as described in sonoporation experiments. Acoustic cavitation was not monitored during sonoporation experiments to avoid high-amplitude scattering from the microcentrifuge tube that would dominate the PCD signal. This allowed isolation of intra- and post-excitation emissions from microbubbles for a unique comparison of cavitation activity between different ultrasound frequencies. The PCD signals (25,000 individual time traces) were collected at each frequency and post-processed in MATLAB. For each FUS frequency group, the signals were processed by summing up the amplitude envelope of all 25,000 individual time traces. This provides information related to when acoustic cavitation activity occurred in time (*i.e.*, collapse times) and the strength of that activity (*i.e.*, cumulative amplitude). The cumulative signals were further analyzed by integrating regions corresponding to intra- and post-excitation emissions. This provides a single value that can be compared across groups to understand the relationship between acoustic cavitation and sonoporation efficiency.

Quantification of bio-effects

Immediately after the FUS exposure, cells were resuspended in fresh cell culture medium and allowed to incubate at room temperature for at least 5 min. Cells were then washed with PBS and resuspended with cold PBS at a concentration of 10^6 cells/mL. Propidium iodide (PI) (Sigma-Aldrich) was added at a concentration of 4 μg/mL to stain non-viable cells. Cells were incubated on ice for 15 min before flow cytometry analysis (FACS Calibur, BD Biosciences, San Jose, CA, USA). Given that the flow cytometer operates at a constant flow rate, data were collected for 1 min to compare the total number of cells counted between control and treatment groups. A reduction in the total number of counted cells indicates that a fraction of cells were destroyed by acoustic cavitation. Cells were analyzed further using the FL1 (*green* channel, FITC–dextran) versus FL3 (*red* channel, PI) scatterplot. Fluorescence thresholds on FL1 and FL3 channels were defined to identify cells that internalized FITC–dextran and were viable, respectively. The reported cell viability was defined as the total number of viable cells divided by the total number of cells in

control exposures. The reported uptake was defined as the total number of viable cells with intracellular FITC–dextran divided by the total number of viable cells. Lastly, the reported uptake efficiency was defined as the total number of viable cells with intracellular FITC–dextran relative to the total number of cells in control exposures. The control exposures were cells that were mixed with FITC–dextran and PSNEs, but not exposed to FUS. All control groups and non-control groups consisted of at least three replicates for determination of cell viability, uptake and uptake efficiency. The values were reported as means ± standard deviations, and a Student's *t*-test was applied to the data; a $p < 0.05$ was considered to indicate significance. A cell proliferation assay (MTT cell proliferation assay, ATCC, Manassas, VA, USA) was also used on treated and non-treated cells to access metabolic activity and cell proliferation after FUS exposure. Cells were resuspended with 1 mL of cell culture medium after washing with PBS and added to 12-well tissue culture plates. Cells were incubated for 24 h, and then the MTT assay was then performed according to the manufacturer's instructions with three replicates for each group. Given that cell proliferation requires viable and functional cells, this assay captures how well the cells recover over time versus the acute effects revealed through PI staining.

RESULTS

As previously reported by Burgess and Porter (2015) and Kopechek et al. (2012), the synthesis steps for PSNEs resulted in a narrow size distribution with a typical mean diameter of 213 ± 31.4 nm and a concentration of 2.0×10^{11} PSNEs/mL. A representative particle size distribution has 10% of the population below 180.1 nm (d_{10} = 180.1) and 90% of the population below 250.4 nm (d_{90} = 250.4). Figure 3 illustrates the results for determination of the ADV threshold of PFP PSNEs at 1 MHz (Fig. 3a), 2.5 MHz (Fig. 3b) and 5 MHz (Fig. 3c). As the peak negative pressure of the FUS was increased, the occurrence of acoustic cavitation events increased until all transmitted pulses generated cavitation. As a comparison, the occurrence of cavitation events in control experiments with PFH PSNEs and no PSNEs remained constant with increasing peak negative pressures. This indicated that vaporized PFP PSNEs were the primary source of cavitation and not the host liquid or the interface between the PSNE and host liquid. It should be noted that acoustic cavitation events were seen in control experiments because of the inability to obtain perfectly clean, filtered water without stabilized gas bodies or imperfections to serve as acoustic cavitation nuclei. This baseline amount of cavitation was low and more evident at lower frequencies, as shown with the increased standard deviations in Figure 3a. The ADV threshold of PSNEs was defined as the peak negative pressure that resulted in ~10% of the PCD signals containing an acoustic cavitation event. Table 1 summarizes the results; the ADV pressure thresholds were 5.6, 5.9 and 4.6 MPa at 1, 2.5 and 5 MHz, respectively.

As illustrated in Figure 2, the PCD signal contained intra- and post-excitation acoustic emissions indicative of microbubble collapse and rebound. Figure 2b is an illustration of the proposed features seen in the PCD signals. Intra-excitation emissions contained scatter at the incident waveform frequency, but also a collapse spike. It is assumed that nucleation occurs during the peak negative cycle of the excitation waveform and the microbubble immediately undergoes growth followed by a collapse during the peak positive cycle. The microbubble then undergoes another growth phase during the subsequent peak negative

cycle, gaining enough momentum to continue through the remainder of the excitation waveform and reach a maximum radius (R_{max}) after passage of the FUS wave. At this point the microbubble experiences an unforced collapse because of the in-rushing liquid surrounding the microbubble. Ensuing post-excitation rebounds and collapses occur after the main collapse from R_{max}. The PCD signals were further analyzed at the ADV pressure threshold for each FUS frequency. Figure 4 illustrates the FUS excitation waveforms, PCD time traces and power spectra of the PCD time traces for each FUS frequency. It was hypothesized that the received passive cavitation signal contains mainly scatter from the incident waveform and broadband emissions radiated during bubble collapse. The broadband energy is evident in all power spectra in Figure 4, as illustrated by the increase in the noise floor by roughly 30–40 dB. Figure 4C does seem to have the most broadband content, perhaps because the collapse strength is strongest at l MHz. Any harmonic content (f_0, $2f_0$, $3f_0$, *etc.*) is from the newly created bubble scattering the incident waveform. The harmonic content in Figure 4F may be due to the increased non-linearity of the incident waveform at 2.5 MHz. As the frequency of the FUS was increased, the occurrence of the first post-excitation spike occurred earlier in time, therefore denoting a shorter collapse time and smaller R_{max}. Using the notation described in Figure 2, Table 1 summarizes the results for the collapse time and estimated R_{max} for each frequency using eqn (1). The estimated R_{max} was 61.7 ± 5.2, 24.9 ± 2.8 and 12.4 ± 2.1 μm at 1, 2.5 and 5 MHz, respectively.

To apply these results to sonoporation experiments, mock exposures were performed using the setup in Figure 1a and FUS parameters used in sonoporation experiments. Figure 5 illustrates the results of the PCD's cumulative signal strength in the intra- and post-excitation regions of the PCD time trace. The integrated cumulative emission strength in both regions decreased with increasing frequency, as outlined in Table 1. Intra-excitation emissions contained scatter from the remainder of the incident waveform, and therefore, the width of the cumulative emission strength decreased with increasing frequency because of shorter acoustic periods. As illustrated in Figure 5b, more signal strength was detected in the post-excitation region at lower frequencies, which suggests more intense microbubble collapses associated with larger microbubble expansions.

As illustrated in Figure 6a, cell viability was inversely related to FUS frequency. Analysis of post-excitation bubble dynamics suggests that bubbles produced by PSNE vaporization undergo larger expansion and collapse more violently at lower frequencies. The cumulative effect of violent bubble collapses can fragment or irreversibly damage cells, dramatically reducing cell viability. Bubble collapse was less intense at higher frequencies, and thus, more cells survived. Reversible disruption of cell membranes, or sonoporation, would provide a pathway for FITC–dextran to diffuse into the cell cytoplasm. Two metrics were defined to compare sonoporation across frequencies: uptake percentage and uptake efficiency. As illustrated in Figure 6b, the uptake percentage exceeded 60% for all FUS frequencies and approached 90% for 1-MHz exposures. However, 1-MHz exposures fragmented and killed more than 50% of the starting cell population. When accounting for cell loss, the uptake efficiency at 1 MHz was approximately 40% and increased with frequency, approaching 70% for 5-MHz exposures (Fig. 6c). These results suggest that the extent of PSNE-nucleated inertial cavitation damage to cell membranes can be modulated through selection of ultrasound frequency.

DISCUSSION

In the work described here, we sought to understand the unique acoustic cavitation properties of PSNEs and their relationship with sonoporation efficiency. PSNEs act as controlled acoustic cavitation nuclei because of their ability to remain in a superheated, metastable state until sufficient negative pressure is reached within the PSNE core to nucleate phase conversion from liquid to vapor (Kripfgans et al. 2000). Recent research has pointed to the suppression of homogeneous nucleation as the likely mechanism for PSNE stability (Mountford and Borden 2016). It is well known that nucleation of vapor bubbles can be suppressed by emulsifying droplets of a volatile liquid in an immiscible non-volatile liquid (Apfel 1971; Avedisian 1985; Shepherd and Sturtevant 1982). PFCs are characterized as being extremely hydrophobic, and therefore, PFC-in-water emulsions are ideal candidates for this scenario (Riess and Riess 2001). Because there are no motes or crevices along the interface of the two fluids, the nucleation process is inhibited until sufficient heating and or a pressure decrease has occurred within the droplet core to cause homogeneous nucleation. This inhibition acts to shift the boiling point of the PFC to the spinodal curve, where researchers have found that submicron PFC droplets can exist up to approximately 90% of their critical temperature (Mountford et al. 2015a, 2015b). From these results, Mountford and Borden (2016) concluded that the energy barrier for homogeneous nucleation was the stabilizing effect of submicron droplets.

The ADV threshold curves in Figure 3 illustrate this controlled nucleation behavior, where significant increases in acoustic cavitation activity occurred over a narrow peak negative pressure range at a fixed temperature. This points to the existence of a critical peak negative pressure that must be reached before ADV can occur. At this threshold, a limited number of PSNEs are subjected to this tensile stress, which led to limited detection of acoustic cavitation events. As the negative pressure was increased, the focal volume that is at or above this threshold increased and, therefore, more acoustic cavitation events were detected. This explains the saturation effect of the ADV threshold curve, where consistent ADV of PSNEs was achieved on every FUS transmit. Given that the PSNE concentration was sufficiently high, the likelihood of PSNEs in the focal volume was high.

Previous researchers have reported that the ADV threshold decreases with increasing frequency for PFC droplets with compositions similar to those of PFP PSNEs (Kripfgans et al. 2000; Schad and Hynynen 2010; Williams et al. 2013). Shpak et al. (2013) were able to uncover the mechanism of ADV of micron-sized droplets using high-speed optical imaging and theoretical predictions. It was determined that ADV was initiated by superharmonic focusing of the ultrasound wave within the droplet, leading to enhanced pressure reduction inside the droplet where ADV is initiated (Shpak et al. 2013). This focusing effect was shown to increase with increasing ultrasound frequency and begins to explain previous studies that reported a decreased ADV threshold with increasing frequency. Other groups have found an increase in the ADV threshold for increasing frequency using PFC droplets with size distributions similar to those of the PSNEs used in this study (Martin et al. 2012; Sheeran et al. 2013; Vlaisavljevich et al. 2015). It is important to note that the study by Shpak et al. (2013) was performed with micron-sized droplets, and it is unknown if the superharmonic focusing mechanism is applicable to submicron droplets. The results of our

study contradict these findings and indicate no frequency dependence on the ADV threshold. We hypothesize that this, along with the ADV threshold curves (Fig. 3), points to the existence of a critical peak negative pressure that must be reached within the PSNE core to initiate ADV, regardless of the acoustic frequency. Future studies will aim to determine if a link exists between the acoustic frequency and ADV threshold of submicron droplets.

A major focus of this work was studying the post-excitation dynamics of microbubbles produced from PSNE vaporization. Numerous other researchers have characterized post-excitation bubble dynamics to better understand single-bubble sonoluminescence (Matula et al. 1998), collapse of lithotripsy and histotripsy bubbles (Cleveland et al. 2000; Kreider et al. 2011; Macoskey et al. 2018; Vlaisavljevich et al. 2015) and inertial cavitation of ultrasound contrast agents (Ammi et al. 2006; King et al. 2010; King and O'Brien 2011). According to the ideal gas law, phase change in PSNEs will result in a microbubble with an equilibrium radius, R_0, that is approximately five times the original diameter of the PSNEs (Sheeran et al. 2011). Assuming that all of the PFC is converted into vapor and there is no influx of water vapor or dissolved gas from the surroundings, a 200-nm-diameter PSNE will transition into a 1-μm-diameter microbubble with a free bubble resonant frequency of ~10 MHz. It has been reported that PFC bubbles formed within the first few cycles of a multicycle vaporization pulse can respond to subsequent cycles (Sheeran et al. 2013). We speculated that the bubbles resulting from PSNE vaporization would have a strong response to later cycles given that the peak negative pressure used in this study (P_{pnp} = 6.5 MPa) far exceeded the inertial cavitation threshold predicted by Apfel and Holland (1991) for a 1-μm gas body (P_{pnp} < 1.0 MPa for f = 1–5 MHz). Moreover, it was hypothesized that the response would vary inversely with frequency. Because the acoustic period is longer at lower frequencies, newly formed microbubbles have more time to grow during the rarefactional period and, as a result, collapse at a later time point. As illustrated by the PCD traces in Figure 4, the acoustic emissions associated with bubble collapse were received at earlier time points as the frequency was increased, thus supporting the hypothesis.

This explanation can be further supported by the concepts put forth by Apfel (1981), who developed an analytical estimate to predict the maximum radius of a microbubble under dynamic forcing of an acoustic wave. This approximation is valid only if the acoustic period is much shorter than the start-up times associated with inertial and viscous effects. Apfel (1981) therefore defined an inertial radius, R_I, where significant growth can occur for microbubbles with an equilibrium radius, R_0, less than R_I:

$$R_I = \frac{1}{4f}\sqrt{\frac{P_A - P_0}{\rho}} \tag{2}$$

where f, P_A, P_0 and ρ are the frequency, acoustic pressure, hydrostatic pressure and liquid density, respectively. At the ADV pressure threshold for each frequency used in this study, R_I is approximately 3.36, 7.62 and 18.56 μm at 5, 2.5 and 1 MHz, respectively. By using the Rayleigh–Plesset equation, Apfel (1981) contended that R_{max} could be estimated as

$$R_{max} = \frac{2}{3\pi f}(P_a - P_0)\sqrt{\frac{2}{\rho P_a}}\left[1 + \frac{2}{3P_0}(P_a - P_0)\right]^{1/3} \tag{3}$$

By use of eqn (3), the R_{max} of microbubbles nucleated from PSNEs can be compared with the values predicted using Rayleigh collapse model in eqn (1), which rely on experimental approximations to define the collapse time. Equation (2) predicts an R_{max} of approximately 74, 31 and 12.5 μm at the ADV thresholds for 1, 2.5 and 5 MHz, respectively. Alternatively, if the predicted R_{max} values calculated with the Rayleigh collapse model (eqn [1]) are used to test if the ADV pressure threshold is the same for each frequency, excellent agreement is found. Using an acoustic pressure of 4.55 MPa for all frequencies leads to R_{max} values of approximately 62, 24.8 and 12.4 μm at 1, 2.5 and 5 MHz, respectively. The agreement with Apfel's (1981) derivation points to the fact that vaporized PSNEs act as prompt inertial cavitation agents. Apfel (1981) goes on to further explain that the "violence" of an inertial cavitation event is tied to the maximum size of the bubble, which corresponds to the energy stored in the liquid before collapse. Equation (2) is independent of the initial microbubble size and depends only on the acoustic pressure and frequency. This assertion may explain the frequency-dependent sonoporation efficiency results. Because the acoustic pressure was fixed, the varying ultrasound frequency has a direct effect on the "violence" of the inertial cavitation activity by changing R_{max}. Thus, there was a transition of inertial cavitation from being too violent at 1 MHz to milder at 5 MHz, and we noted a corresponding increase in cell viability.

Studies with micron-sized PFC droplets have shown contradictory results to rapid expansion and collapse of microbubbles as seen with ADV of submicron droplets. Stable bubble oscillations and non-inertial collapse have been consistently seen using optical and acoustic measurement systems (Sheeran et al. 2013; Shpak et al. 2013). PFC droplets with diameters ranging from 1 to 10 μm would result in bubbles with diameters of approximately 5–50 μm and resonant frequencies of 1.35–0.1 MHz, respectively. In the typical ultrasound frequency range of 1–10 MHz, these microbubbles will not respond rapidly to an ultrasound pulse. In this situation, the bubble would be insonified above its resonant frequency in an inertia-controlled regime. This would explain the studies by Fabiilli et al. (2009) that have shown ADV of micron-sized PFC droplets can occur with or without inertial cavitation. For the large bubbles formed after ADV, inertia effects dominate the initial growth, which increases the inertial cavitation threshold. It takes much more force (*i.e.*, pressure differential across the bubble wall), on much longer time scales (*i.e.*, acoustic period length), to achieve significant microbubble expansion.

Further acoustic cavitation control could be achieved through the use of different PFC cores. Researchers have found that PSNE can be formulated with PFCs that have varying boiling points, which changes the pressure threshold for ADV (Sheeran et al. 2012). For higher-boiling PFCs, the ADV threshold would increase and provide controlled activation of more violent inertial cavitation. Conversely, lower-boiling PFCs could be used to reduce the required peak negative pressure and decrease the intensity of inertial cavitation or completely eliminate it (Sheeran et al. 2014). This could be important for applications that utilize PSNEs for contrast-enhanced ultrasound imaging (Williams et al. 2013). The combination of lower peak negative pressures and higher frequencies (>5 MHz) could provide controlled activation of stable cavitation for utilization of non-linear ultrasound imaging modes. It was also recently found that vaporizable emulsions made with low-boiling-point PFC could be used for sonoporation of cultured cells (Fix et al. 2017). The

results reported in this study suggest that efficient and non-lethal sonoporation is achievable through a combination of vaporizable PFC nanoemulsions and relatively high-frequency ultrasound (≥5 MHz). This is counterintuitive to conventional thought in which lower frequencies are utilized to increase the likelihood of inertial cavitation. However, as reported in this study, the use of lower frequencies can lead to more intense inertial cavitation, which ultimately kills more cells and reduces sonoporation efficiency. Collectively, these studies indicate the potential for tailoring cavitation-mediated sonoporation and associated bio-effects through rational selection of emulsion PFC cores and acoustic parameters, particularly excitation frequency. Future studies will focus on the translation of these concepts to *in vivo* scenarios with medium properties similar to blood and tissue.

CONCLUSIONS

Controlled inception of inertial cavitation can be obtained through the use of FUS and PSNEs. PSNEs remain in a metastable state until sufficient negative pressure is reached within the PSNE core to trigger homogenous nucleation. With the PSNE composition used in this study, the ADV process occurs over a narrow peak negative pressure range, and the subsequent microbubble dynamics are predictable based on the FUS frequency. All the frequencies used in this study led to prompt nucleation of inertial cavitation above the ADV threshold, with lower frequencies causing more extensive microbubble expansion. This led to a drop in sonoporation efficiency at lower frequencies because of excessive cellular damage caused my highly energetic inertial collapse. These results highlight the need for acoustic cavitation control and indicate that not all inertial cavitation activity is the same. Additionally, other therapeutic ultrasound techniques may benefit from the unique acoustic cavitation properties of PSNE.

Acknowledgments—

This work was supported in part by National Institutes of Health Grants R03EB015089, R01EB016102 and R25CA153955.

REFERENCES

Ammi AY, Cleveland RO, Mamou J, Wang GI, Bridal SL, O'Brien WD. Ultrasonic contrast agent shell rupture detected by inertial cavitation and rebound signals. IEEE Trans Ultrason Ferroelectr Freq Control 2006;53:126–136. [PubMed: 16471439]

Apfel RE. A novel technique for measuring the strength of liquids. J Acoust Soc Am 1971;49:145.

Apfel R Acoustic cavitation prediction. J Acoust Soc Am 1981;69: 1624–1633.

Apfel RE, Holland CK. Gauging the liklihood of cavitation from short-pulse, low-duty cycle diagnostic ultrasound. Ultrasound Med Biol 1991;17:179–185. [PubMed: 2053214]

Avedisian CT. The homogeneous nucleation limits of liquids. J Phys Chem Ref Data 1985;14:695–729.

Burgess MT, Porter TM. Acoustic cavitation-mediated delivery of small interfering ribonucleic acids with phase-shift nano-emulsions. Ultrasound Med Biol 2015;41:2191–2201. [PubMed: 25979417]

Carugo D, Owen J, Crake C, Lee JY, Stride E. Biologically and acoustically compatible chamber for studying ultrasound-mediated delivery of therapeutic compounds. Ultrasound Med Biol 2015;41: 1927–1937. [PubMed: 25922133]

Cleveland RO, Sapozhnikov OA, Bailey MR, Crum LA. A dual passive cavitation detector for localized detection of lithotripsy-induced cavitation *in vitro*. J Acoust Soc Am 2000;107:1745–1758. [PubMed: 10738826]

Coussios CC, Roy RA. Applications of acoustics and cavitation to non-invasive therapy and drug delivery. Annu Rev Fluid Mech 2008;40: 395–420.

Dixon AJ, Dhanaliwala AH, Chen JL, Hossack JA. Enhanced intracellular delivery of a model drug using microbubbles produced by a microfluidic device. Ultrasound Med Biol 2013;39:1267–1276. [PubMed: 23643062]

Fabiilli ML, Haworth KJ, Fakhri NH, Kripfgans OD, Carson PL, Fowlkes JB. The role of inertial cavitation in acoustic droplet vaporization. IEEE Trans Ultrason Ferroelectr Freq Control 2009;56:1006–1017. [PubMed: 19473917]

Fan Z, Liu H, Mayer M, Deng CX. Spatiotemporally controlled single cell sonoporation. Proc Natl Acad Sci USA 2012;109:16486–16491. [PubMed: 23012425]

Fix SM, Novell A, Yun Y, Dayton PA, Arena CB. An evaluation of the sonoporation potential of low-boiling point phase-change ultrasound contrast agents *in vitro*. J Ther Ultrasound 2017;5:7. [PubMed: 28127427]

Hallow DM, Mahajan ADU, McCutchen TE, Prausnitz MR. Measurement and correlation of acoustic cavitation with cellular bioeffects. Ultrasound Med Biol 2006;32:1111–1122. [PubMed: 16829325]

Holland CK, Apfel RE. An improved theory for the prediction of microcavitation thresholds. IEEE Trans Ultrason Ferroelectr Freq Control 1989;36:204–208. [PubMed: 18284969]

King DA, O'Brien WD. Comparison between maximum radial expansion of ultrasound contrast agents and experimental postexcitation signal results. J Acoust Soc Am 2011;129:114–121. [PubMed: 21302993]

King DA, Malloy MJ, Roberts AC, Haak A, Yoder CC, O'Brien WD. Determination of postexcitation thresholds for single ultrasound contrast agent microbubbles using double passive cavitation detection. J Acoust Soc Am 2010;127:3449–3455. [PubMed: 20550244]

Kopechek JA, Zhang P, Burgess MT, Porter TM. Synthesis of phase-shift nanoemulsions with narrow size distributions for acoustic droplet vaporization and bubble-enhanced ultrasound-mediated ablation. J Vis Exp 2012;67:e4308.

Kreider W, Crum LA, Bailey MR, Sapozhnikov OA. Observations of the collapses and rebounds of millimeter-sized lithotripsy bubbles. J Acoust Soc Am 2011;130:3531–3540. [PubMed: 22088027]

Kripfgans OD, Fowlkes JB, Miller DL, Eldevik OP, Carson PL. Acoustic droplet vaporization for therapeutic and diagnostic applications. Ultrasound Med Biol 2000;26:1177–1189. [PubMed: 11053753]

Kudo N, Okada K, Yamamoto K. Sonoporation by single-shot pulsed ultrasound with microbubbles adjacent to cells. Biophys J 2009;96:4866–4876. [PubMed: 19527645]

Lai CY, Wu CH, Chen CC, Li PC. Quantitative relations of acoustic inertial cavitation with sonoporation and cell viability. Ultrasound Med Biol 2006;32:1931–1941. [PubMed: 17169705]

Leighton T The acoustic bubble. London: Academic Press; 1994.

Lentacker I, De Cock I, Deckers R, De Smedt SC, Moonen CTW. Understanding ultrasound induced sonoporation: Definitions and underlying mechanisms. Adv Drug Deliv Rev 2014;72:49–64. [PubMed: 24270006]

Liu Y, Yan J, Prausnitz MR. Can ultrasound enable efficient intracellular uptake of molecules? A retrospective literature review and analysis. Ultrasound Med Biol 2012;38:876–888. [PubMed: 22425381]

Macoskey J, Choi S, Hall T, Vlaisavljevich E, Lundt J, Lee F, Johnsen E, Cain C, Xu Z. Using the cavitation collapse time to indicate the extent of histotripsy-induced tissue fractionation. Phys Med Biol 2018;63 055013. [PubMed: 29424711]

Martin AL, Seo M, Williams R, Belayneh G, Foster FS, Matsuura N. Intracellular growth of nanoscale perfluorocarbon droplets for enhanced ultrasound-induced phase-change conversion. Ultrasound Med Biol 2012;38:1799–1810. [PubMed: 22920544]

Matula TJ, Hallaj IM, Cleveland RO, Crum LA, Moss WC, Roy RA. The acoustic emissions from single-bubble sonoluminescence. J Acoust Soc Am 1998;103:1377–1382.

Mountford PA, Borden MA. On the thermodynamics and kinetics of superheated fluorocarbon phase-change agents. Adv Colloid Interface Sci 2016;237:15–27. [PubMed: 27574721]

Mountford PA, Smith WS, Borden MA. Fluorocarbon nanodrops as acoustic temperature probes. Langmuir 2015a;31:10656–10663. [PubMed: 26359919]

Mountford PA, Thomas AN, Borden MA. Thermal activation of superheated lipid-coated perfluorocarbon drops. Langmuir 2015b;31: 4627–4634. [PubMed: 25853278]

Neppiras EA. Acoustic cavitation. Phys Rep 1980;61:163–251.

Ohl C, Arora M, Ikink R, De Jong N, Versluis M, Delius M. Sonoporation from jetting cavitation bubbles. Biophys J 2006;91:4285–4295. [PubMed: 16950843]

Rayleigh L On the pressure developed in a liquid during the collapse of a spherical cavity. Phil Mag 1917;34:94–98.

Riess JG, Riess JG. Oxygen carriers ("blood substitutes")—Raison d'etre, chemistry, and some physiology. Chem Rev 2001;101:2797–2919. [PubMed: 11749396]

Schad K, Hynynen K. In vitro characterization of perfluorocarbon droplets for focused ultrasound therapy. Phys Med Biol 2010;55: 4933–4947. [PubMed: 20693614]

Sengupta A, Kelly SC, Dwivedi N, Thadhani N, Prausnitz MR. Efficient intracellular delivery of molecules with high cell viability using nanosecond-pulsed laser- activated carbon nanoparticles. ACS Nano 2014;2889–2899. [PubMed: 24547946]

Seya PM, Fouqueray M, Ngo J, Poizat A, Inserra C, Bera J-C. Sonoporation of adherent cells using regulated ultrasound cavitation conditions. Ultrasound Med Biol 2015;41:1008–1019. [PubMed: 25701522]

Sheeran PS, Wong VP, Luois S, McFarland RJ, Ross WD, Feingold S, Matsunaga TO, Dayton PA. Decafluorobutane as a phase-change contrast agent for low-energy extravascular ultrasonic imaging. Ultrasound Med Biol 2011;37:1518–1530. [PubMed: 21775049]

Sheeran P, Luois S, Mullin L, Matsunaga T, Dayton P. Design of ultrasonically-activatable nanoparticles using low boiling point perfluorocarbons. Biomaterials 2012;33:3262–3269. [PubMed: 22289265]

Sheeran PS, Matsunaga TO, Dayton PA. Phase-transition thresholds and vaporization phenomena for ultrasound phase-change nanoemulsions assessed *via* high-speed optical microscopy. Phys Med Biol 2013;58:4513–4534. [PubMed: 23760161]

Sheeran PS, Matsunaga TO, Dayton PA, Hill C. Phase change events of volatile liquid perfluorocarbon contrast agents produce unique acoustic signatures. Phys Med Biol 2014;59:379–401. [PubMed: 24351961]

Shepherd JE, Sturtevant B. Rapid evaporation at the superheat limit. J Fluid Mech 1982;121:379–402.

Shpak O, Kokhuis TJA, Luan Y, Lohse D, De Jong N, Fowlkes B, Fabiilli M. Ultrafast dynamics of the acoustic vaporization of phase-change microdroplets. J Acoust Soc Am 2013;134:1610–1621. [PubMed: 23927201]

Song KH, Fan AC, Brlansky JT, Trudeau T, Gutierrez-Hartmann A, Calvisi ML, Borden MA. High efficiency molecular delivery with sequential low-energy sonoporation bursts. Theranostics 2015;5:1419–1427. [PubMed: 26681986]

Sundaram J, Mellein BR, Mitragotri S. An experimental and theoretical analysis of ultrasound-induced permeabilization of cell membranes. Biophys J 2003;84:3087–3101. [PubMed: 12719239]

Vlaisavljevich E, Aydin O, Durmaz Y, Lin K, Fowlkes B, El Sayed M, Xu Z. Effects of ultrasound frequency on nanodroplet-mediated histotripsy. Ultrasound Med Biol 2015;41:2135–2147. [PubMed: 25959056]

Van Wamel A, Kooiman K, Harteveld M, Emmer M, Folkert J, Versluis M, De Jong N. Vibrating microbubbles poking individual cells: Drug transfer into cells *via* sonoporation. J Control Release 2006;112:149–155. [PubMed: 16556469]

Williams R, Wright C, Cherin E, Reznik N, Lee M, Gorelikov I, Foster FS, Matsuura N, Burns PN. Characterization of submicron phase-change perfluorocarbon droplets for extravascular ultrasound imaging of cancer. Ultrasound Med Biol 2013;39:475–489. [PubMed: 23312960]

Zhang P, Porter T. An *in vitro* study of a phase-shift nanoemulsiona: potential nucleation agent for bubble-enhanced HIFU tumor ablation. Ultrasound Med Biol 2010;36:1856–1866. [PubMed: 20888685]

Zhou Y, Kumon R, Cui J, Deng C. The size of sonoporation pores on the cell membrane. Ultrasound Med Biol 2009;35:1756–1760. [PubMed: 19647924]

Zhou Y, Yang K, Cui J, Ye J, Deng C. Controlled permeation of cell membrane by single bubble acoustic cavitation. J Control Release 2012;157:103–111. [PubMed: 21945682]

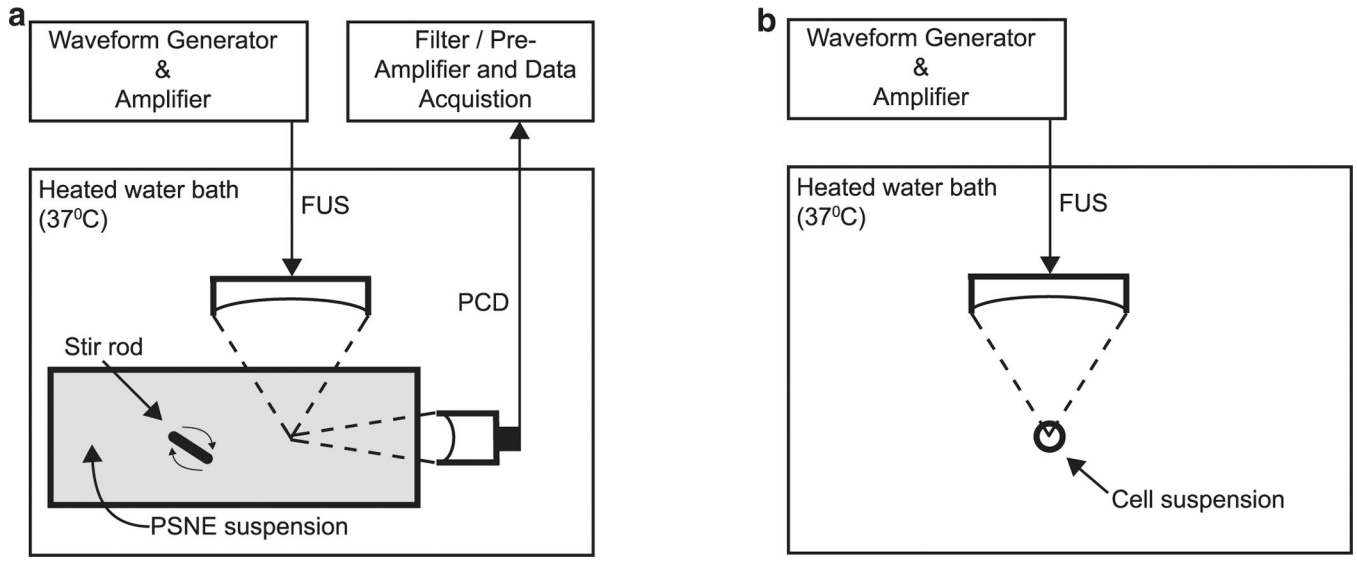

Fig. 1.

Experimental setups used for detecting frequency-dependent acoustic emissions (a) during and after ADV of PSNEs and (b) frequency-dependent sonoporation efficiency. (a) FUS transducers were submerged in a heated bath of degassed, de-ionized water and used to interrogate a PSNE suspension (10^9 PSNEs/mL) with short pulses of FUS (5 cycles, 4–8 MPa peak negative pressure and 100-Hz pulse repetition frequency). Acoustic cavitation emissions were captured with a broadband PCD and post-processed to understand the dynamics of microbubbles derived from PSNEs after ADV. (b) A cell suspension containing cancer cells, PSNEs (10^9/mL) and mock biomolecule FITC-dextran (10 μM) were placed in a microcentrifuge tube and submerged in a heated bath of degassed, de-ionized water. FUS (5 cycles, 6.5-MPa peak negative pressure, 250-Hz pulse repetition frequency and 100-s treatment duration) was then used to vaporize PSNEs and promote acoustic cavitation activity within the cell suspension for intracellular delivery of FITC-dextran. ADV = acoustic droplet vaporization; FITC = fluorescein isothiocyanate; FUS = focused ultrasound; PCD = passive cavitation detector; PSNE = phase-shift nanoemulsions.

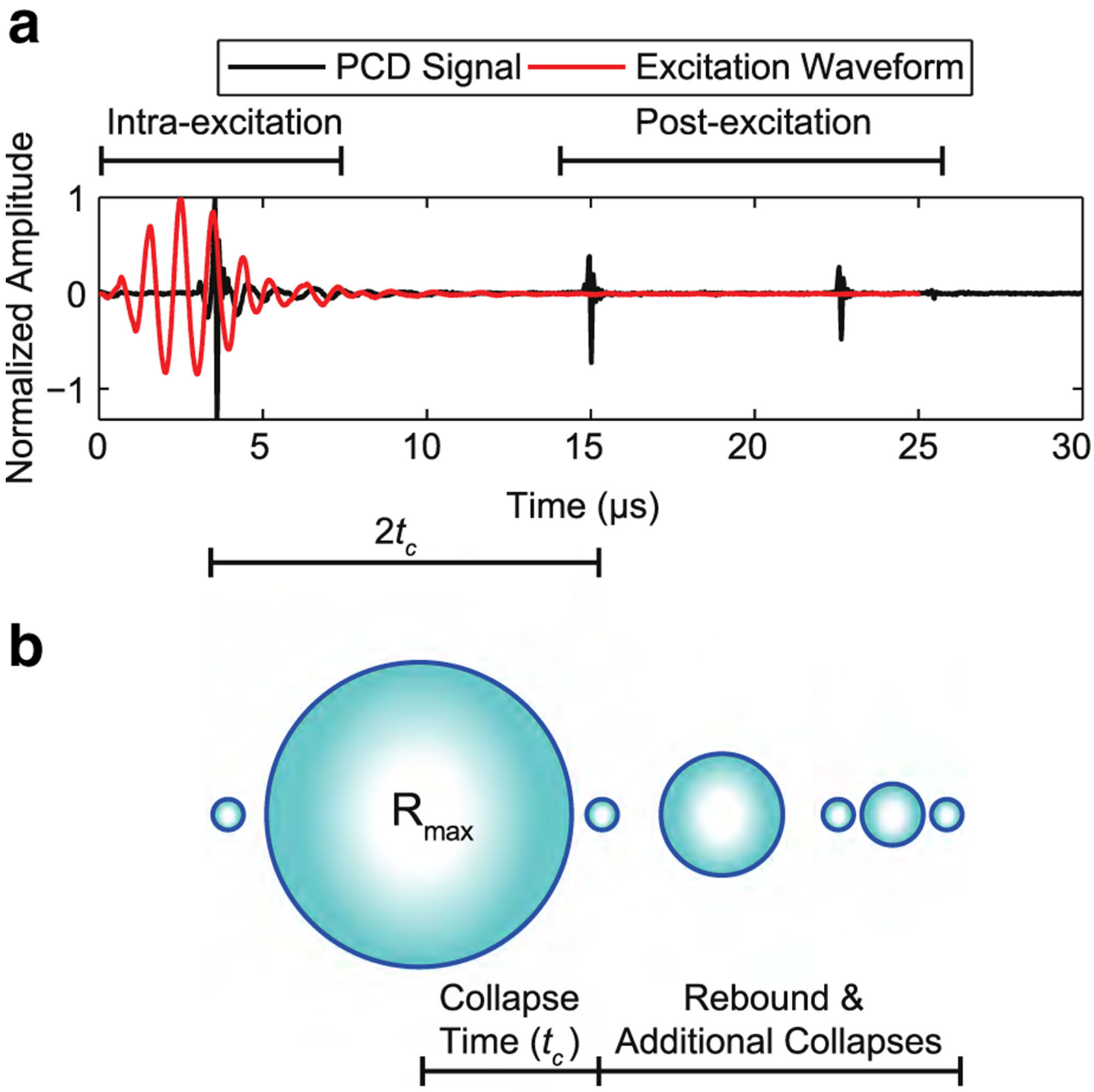

Fig. 2.

(a) An example time trace from the passive cavitation detector revealing intra- and post-excitation acoustic emissions relative to the focused ultrasound excitation waveform during the acoustic droplet vaporization of a single phase-shift nanoemulsion. The excitation waveform was a 1-MHz pulse at a peak negative pressure of 5.6 MPa. The waveform was measured using a calibrated hydrophone at a lower peak negative pressure (~1 MPa). (b) Hypothesized microbubble dynamics in relation to the temporal characteristics of the time trace. It is theorized that the microbubbles undergo rapid growth to a maximum radius (R_{max}), followed by multiple collapses and rebounds after acoustic droplet vaporization of

phase-shift nanoemulsions. The collapse time (t_C) is defined as the time between the first intra-excitation collapse spike to the first post-excitation collapse spike.

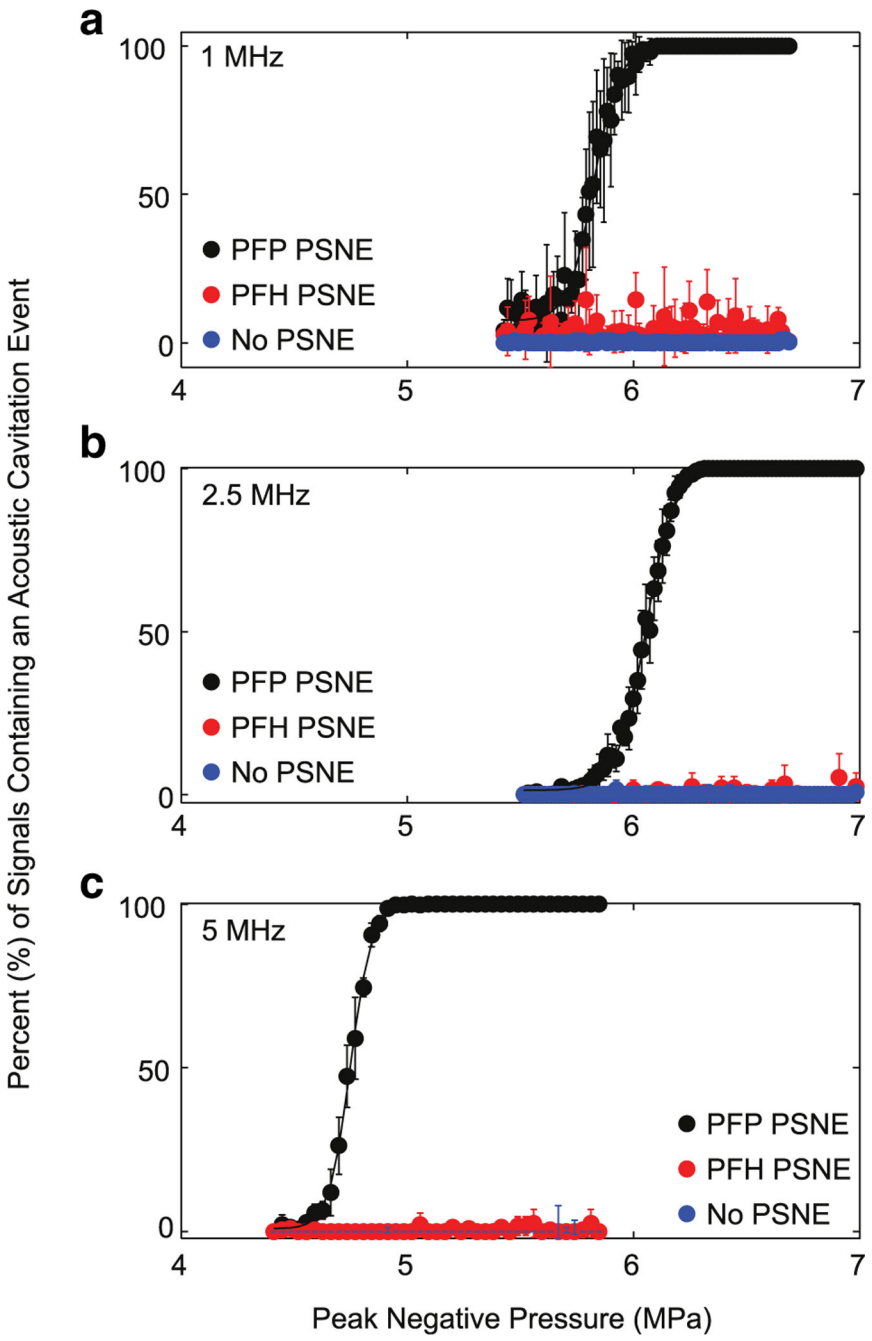

Fig. 3.

(a-c) Acoustic droplet vaporization (ADV) threshold of phase-shift nanoemulsions (PSNE) as a function of the focused ultrasound (FUS) peak negative pressure at 1 MHz (a), 2.5 MHz (b), and 5 MHz (c). Using the experimental set-up in Figure 1a, a PSNE suspension (10^9 PSNE/mL) was interrogated with pulsed FUS (5 cycles, 4–8 MPa peak negative pressure and 100-Hz pulse repetition frequency), and acoustic cavitation emissions were simultaneously recorded with a broadband passive cavitation detector. PFP and PFH PSNEs were interrogated along with water (no PSNE) as a control. Results are depicted as the percentage of signals containing an acoustic cavitation event versus the peak negative

pressure of the focused ultrasound. A total of 100 individual time traces were captured at each pressure step for post-processing. The ADV threshold was defined as the peak negative pressure that resulted in 10% of the signals containing acoustic cavitation events and was 5.6, 5.9 and 4.6 MPa at 1, 2.5 and 5 MHz, respectively. PFH = perfluorohexane; PFP = perfluropentane; PSNEs = phase-shift nanoemulsions.

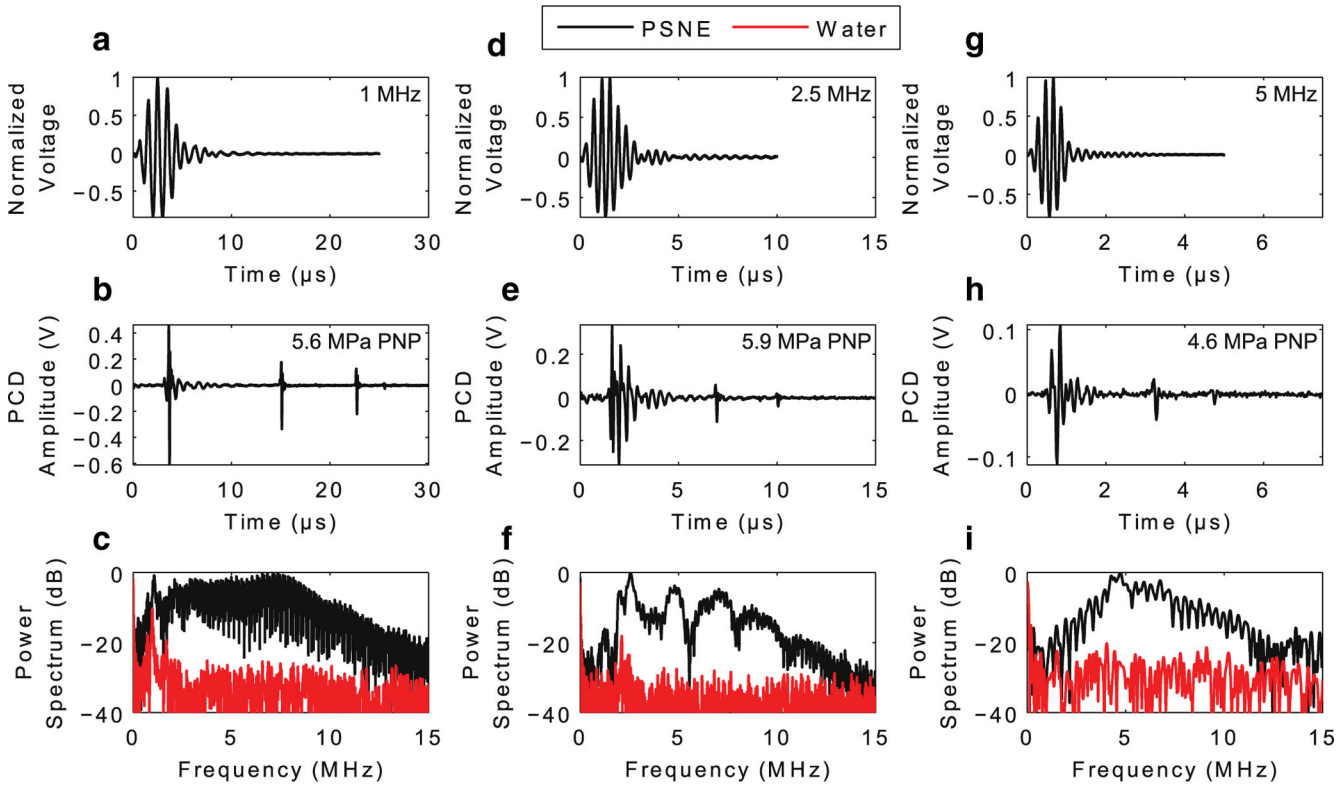

Fig. 4.

Acoustic emissions from individual PSNEs after acoustic droplet vaporization with focused ultrasound at frequencies of (a–c) 1 MHz, (d–f) 2.5 MHz and (g–i) 5 MHz. (a, d, g) Focused ultrasound waveform for each frequency as measured with a needle hydrophone at a peak negative pressure of ~1 MPa. (b, e, h) Recorded time traces detected by the passive cavitation detector during and after acoustic droplet vaporization of single PSNEs. (c, f, i) Frequency content of the recorded time traces. The focused ultrasound pulse parameters were 5 cycles at peak negative pressures of 5.6, 5.9 and 4.6 MPa for 1, 2.5 and 5 MHz, respectively. PNP = peak negative pressure; PSNEs = phase-shift nanoemulsions.

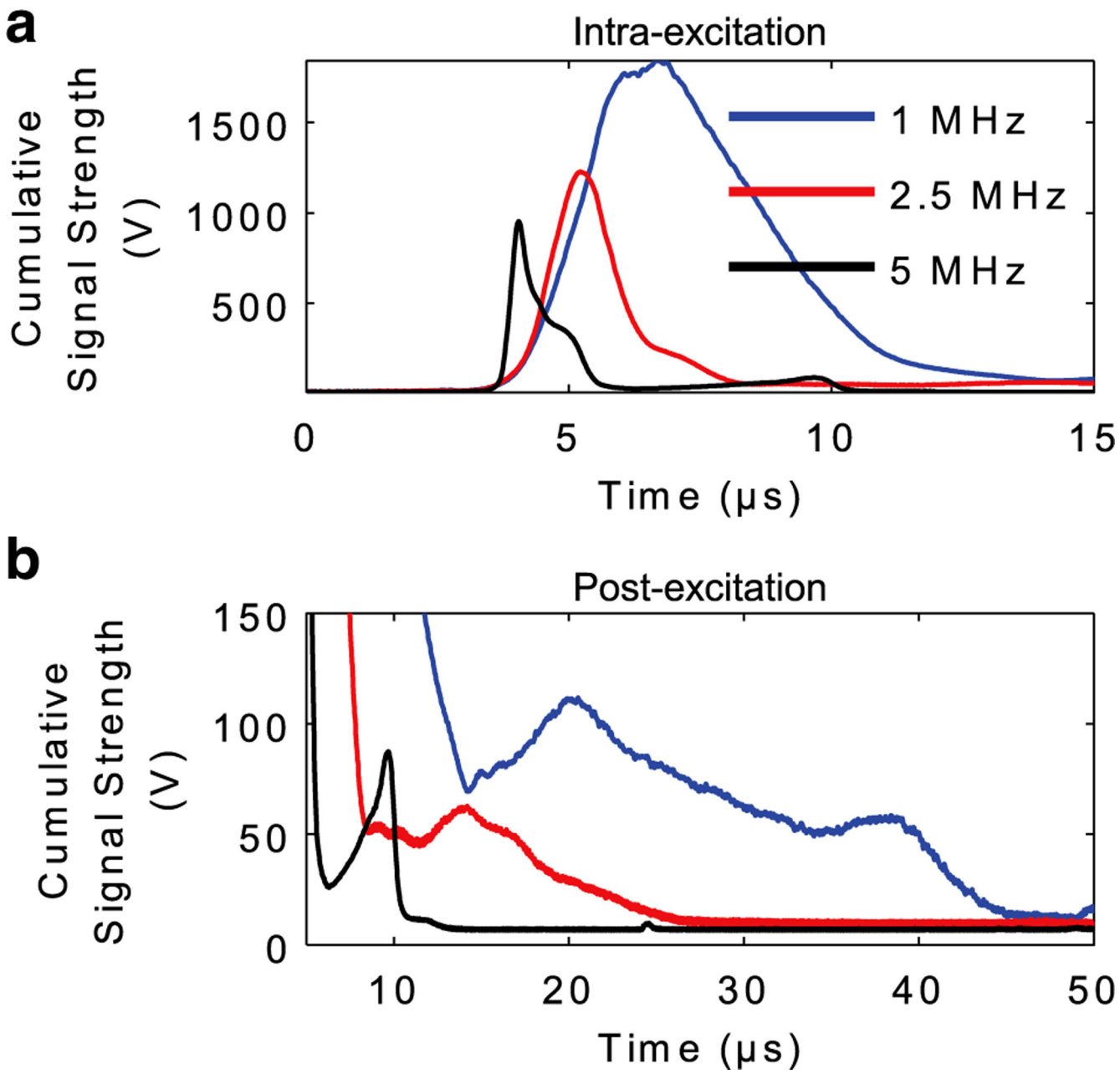

Fig. 5.

Cumulative acoustic cavitation emissions during mock sonoporation experiments. PSNEs (10^9/mL) were interrogated with focused ultrasound using the experimental setup in Figure 1a and FUS parameters used in sonoporation experiments (5-cycle pulse, 6.5-MPa peak negative pressure, 250-Hz pulse repetition frequency and 100-s treatment duration). Cumulative signal strength from intra-excitation and post-excitation emissions was isolated by summing up the amplitude envelope of all 25,000 individual time traces. This provides information related to when acoustic cavitation activity occurred in time (*i.e.*, collapse times) and the strength of that activity (*i.e.*, cumulative amplitude). PSNE = phase-shift nanoemulsion.

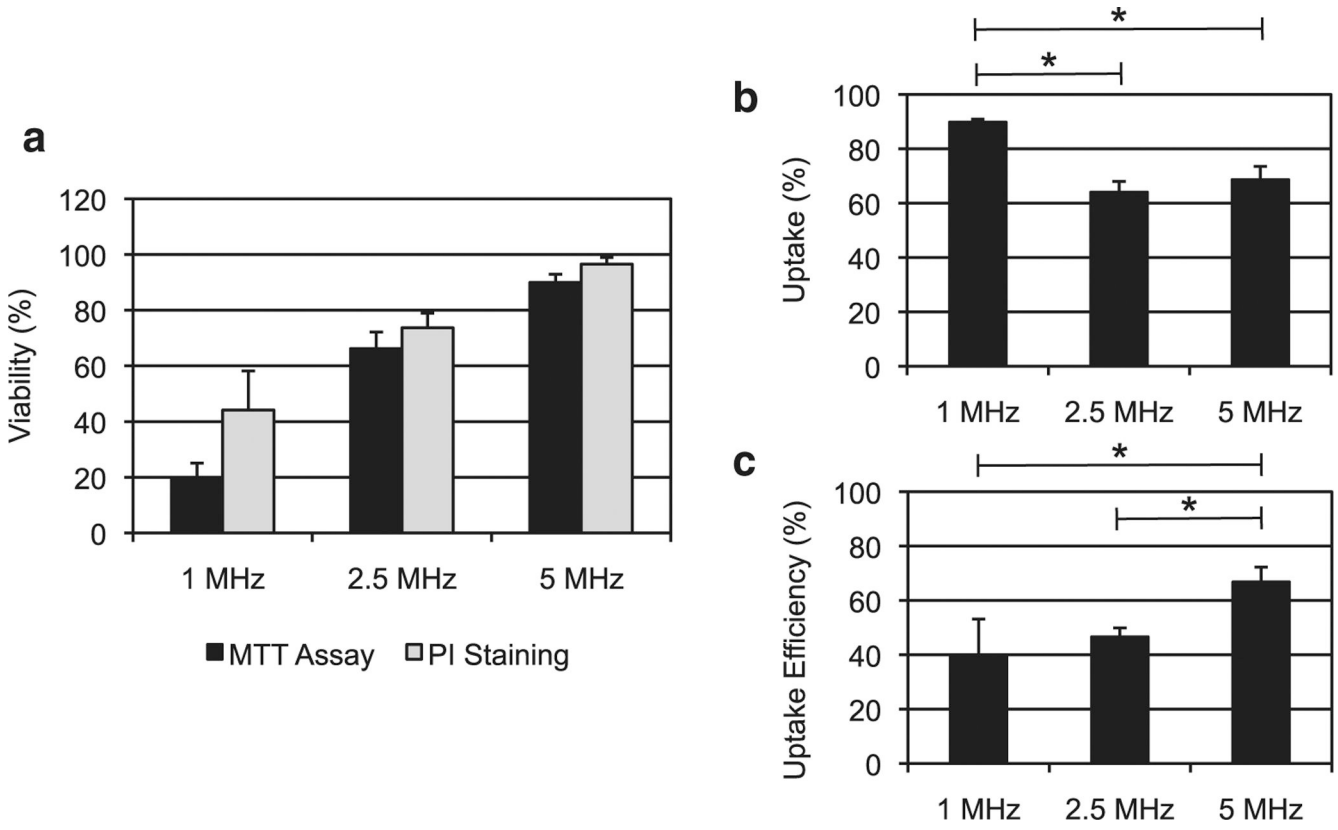

Fig. 6.

Relationship between the FUS frequency and outcome of sonoporation experiments using PSNEs. The FUS parameters were fixed at 5 cycles, 6.5-MPa peak negative pressure, 250-Hz pulse repetition frequency and 100-s exposure duration. (A) Cell viability measured using a cell proliferation assay 24 h after focused ultrasound exposure (MTT assay) or immediately after the exposure with flow cytometry and PI staining. (B) Percentage of viable cells exhibiting uptake of mock biomolecule fluorescein isothiocyanate-dextran (20 kDa) after FUS exposure. (C) Uptake efficiency, which is the percentage of viable cells with uptake relative to the total number of initial cells, at the three FUS frequencies. FUS = focused ultrasound; PI = propidium iodide; PSNEs = phase-shift nanoemulsions.

Table 1.

Frequency-dependent acoustic cavitation properties of phase-shift nanoemulsions

Frequency (MHz)	ADV threshold (peak negative pressure) (MPa)	Collapse time, t_c (s)	Estimated R_{max} (μm)	Integrated cumulative emission strength (V·s)	Integrated cumulative emission strength post-excitation (V·s)
1	5.6	5.59 ± 0.47	61.7 ± 5.2	4.91×10^5	1.08×10^5
2.5	5.9	2.25 ± 0.25	24.9 ± 2.8	1.52×10^5	0.36×10^5
3	4.6	1.125 ± 0.19	12.4 ± 2.1	0.68×10^5	0.27×10^5